DOI: 10.1021/ma900475h

Macromolecules
ARTICLE

Epitaxially Dominated Crystalline Morphologies of the γ-Phase in Isotactic Polypropylene

Yan Cao,[†,‡] Ryan M. Van Horn,[†] Chi-Chun Tsai,[†] Matthew J. Graham,[†] Kwang-Un Jeong,[§] Bojie Wang,[†] Finizia Auriemma,[⊥] Claudio De Rosa,[⊥] Bernard Lotz,*[,∥] and Stephen Z. D. Cheng*[,†]

[†]*Institute of Polymer Science and Polymer Engineering, Department of Polymer Science, The University of Akron, Akron, Ohio 44325-3909,* [‡]*Department of Polymer Science and Engineering, South China University of Technology, Guangzhou 510640, China,* [§]*Department of Polymer Nano Science and Technology, Chonbuk National University, Jeonju, Korea,* [⊥]*Dipartimento Chim Paolo Corradini, University of Naples Federico 2, Complesso Monte S Angelo, Via Cintia, I-80126 Naples, Italy, and* [∥]*Institut Charles Sadron, 23, Rue du Loess, Strasbourg 67034, France*

Received March 4, 2009; Revised Manuscript Received April 21, 2009

ABSTRACT: In the past, the crystallographic relationship between the γ-phase and the α-phase in isotactic polypropylene (i-PP) was extensively studied and established *via* i-PP oligomers of which the γ-phase can be formed at atmospheric pressure. We attempt to investigate how the epitaxial domination of the crystal morphologies takes place in the γ-phase of chain-folded crystals using high molecular weight i-PP samples with a controlled number of stereodefects. These specifically synthesized samples favor the isothermal growth of the γ-phase crystals from a thin film melt at 100−140 °C at atmospheric pressure. It is known that the γ-phase unit cell has the very unique characteristic of an orthorhombic lattice with alternating stem orientations in every two stem layers along the *c*-axis. Due to the specific epitaxial growth of the γ-phase on the elongated α-phase single crystals, two different morphologies were identified *via* transmission electron and atomic force microscopies (TEM and AFM). The first γ-phase crystalline morphology is needle-like. The selected area electron diffraction (SAED) results showed that either the [$\bar{1}$10] or [110] zone axis was parallel to the thin film normal, and the needle direction was along the *c*-axis of the γ-phase. The epitaxial growth of this type of γ-phase crystal was generated from the stem direction in the initial α-phase single crystal being parallel to the thin film (and thus, the lamellar) normal. In this case, the stem length of the α-phase single crystal provided a limit for the growth of the γ-phase to develop toward the thin film normal. On the other hand, the stem length oriented at ±80° away from the film normal in the γ-phase crystal was limited by the folded chain crystal growth kinetics, which is proportional to the reciprocal supercooling. These two factors thus resulted in the formation of these peculiar needle-like crystals. The second γ-phase crystalline morphology was "flat" lamellae. The SAED results indicated that the chain orientations in the "flat" lamellae were tilted at ± 40° from the thin film normal within the *ab*-plane of the γ-phase. Macroscopically, growth of the "flat" lamellae was thermodynamically more stable compared with the needle-like crystals due to their larger crystal size. On the basis of the tilted SAED and dark field results from TEM, the microscopic formation mechanism of this morphology revealed that the initial α-phase single crystal had to have a stem orientation tilted ± 25° away from the thin film normal within the *ac*-plane around the *b*-axis. Therefore, the epitaxial growth of the γ-phase on the *ac*-plane of the α-phase did not possess a chain orientation of ± 40° from the thin film normal. The final "flat" lamellar γ-phase crystals might have resulted from a continuous twist of the chain orientation from +25°/−55° or −25°/+55° to ±40° from the thin film normal.

Introduction

Structural and morphological evidence of the polymorphic behavior in isotactic polypropylene (i-PP) has long been known but subjected to extensive investigations.[1−9] The two main crystalline polymorphs observed in i-PP are the α- and β-phases. The α-phase of i-PP crystals was reported more than half a century ago, as established by Natta and Corradini.[10] It has a monoclinic unit cell with $a = 0.665$ nm, $b = 2.096$ nm, $c = 0.65$ nm, and $\beta = 99.62°$. Although the structure of the β-phase of i-PP was discovered in 1959,[1] it proved puzzling for the next 35 years. Then, in 1994, the β-phase was determined to possess a frustrated trigonal unit cell with $a = b = 1.101$ nm, $c = 0.65$ nm.[11,12] Furthermore, i-PP also has another crystal polymorph, the γ-phase.

*To whom correspondence should be addressed. E-mail: (S.Z.D.C.) scheng@uakron.edu; (B.L.) lotz@ics.u-strasbg.fr.

The γ-phase structure is closely associated with the α-phase through epitaxial crystallographic association.[13,14] In 1961, Addink and Beintema reported wide-angle X-ray diffraction (WAXD) powder patterns of a low molecular weight (MW) i-PP. This pattern was later described to be the γ-phase.[1] In 1968, Morrow and Newman proposed that the γ-phase structure in i-PP had a triclinic unit cell. However, later studies showed that their γ-phase structure does not exist at a free energy minimum and thus, it cannot be stabilized, bringing speculation to their assertion.[15] In order to obtain the pure γ-phase one of the following four ways are usually required: crystallization in the melt under elevated pressures (about 5000 atm);[16−20] crystallization of low MW i-PP at atmospheric pressure;[13,14,21] crystallization of high MW i-PP samples containing a non-negligible amount of *rr* stereodefects;[22,23] or in copolymers of i-PP with small amounts of short chain branches (such as ethylene or butene) prepared using metallocene catalysts.[24]

 Published on Web 05/12/2009

The correct structure of the γ-phase was reported in 1989.[25] Brückner and Meille refined the γ-phase crystal structure utilizing the Rietveld method on WAXD results collected at a low temperature (−120 °C).[26] On the basis of this analysis, they proposed a peculiar crystal structure with nonparallel stem axes within the unit cell. It is a face-centered orthorhombic lattice (a = 0.854 nm, b = 0.993 nm, c = 4.241 nm). This has not been observed in any other macromolecular crystal system. Stems in the crystal orient parallel to the *ab*-plane diagonals, and their orientation alternates by 80° or 100° every two layers. Within these two layers (one building block), the stems possess antichiral helices (opposite helical handedness) but the same orientation. The stem axes in the neighboring building blocks are tilted 80° or 100°. The chirality of the helical stems in these adjacent layers is always identical. The stem packing in the γ-phase is shown schematically in Figure 1a.[25] This stem orientation change occurs on the molecular level, so it is called "molecular epitaxy." A three-dimensional (3D) crystal structure of the γ-phase of i-PP is shown in Figure 1b.[26]

In all of the polymorphs of i-PP, the rotational symmetry of the stems is always 3-fold with both left- and right-handed helical conformations. Therefore, the different chain packing is the determining factor for the appearance of these polymorphs. In the α-phase of i-PP, an alternation of the helical handedness along the *b*-axis direction is observed. When we consider the methyl group orientation in the stem conformations, two subphase structures can be identified as the α_1 and α_2 phases.[27,28] The packing of stem helices is such that each helix interacts with neighboring stem helices of opposite hand located in adjacent layers. Each 3_1 helix has one methyl group pointing in either the $+b$ or the $-b$ direction, and the other two methyl groups are in a plane perpendicular to the *b*-axis. This creates two possible growth (contact) faces as seen from the $+b$ and $-b$ directions.[29] One is called the "four-methyl face", and the other is the "five-methyl face".

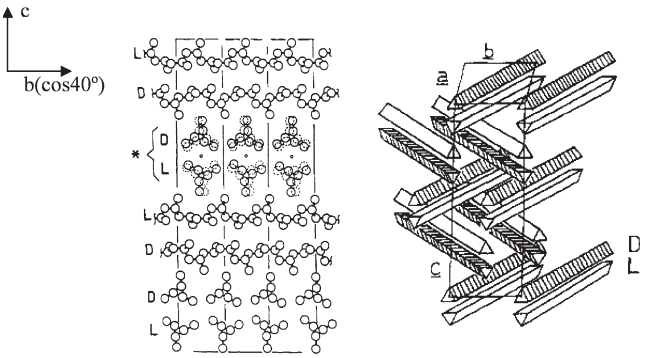

Figure 1. (a) Crystal structure of the γ-phase of i-PP as determined by Brückner and Meille. Reprinted from ref 25 with permission. Copyright 1989 Nature Publishing Group. (b) A 3D crystal structure of the γ-phase of i-PP. D (marked with stripe) and L (without marking) have different helical chiralities. Reprinted from ref 26 with permission. Copyright 1990.

The five-methyl growth face possesses a striking difference in density of exposed methyl groups compared with the four-methyl growth face. It has been shown by Brückner and Meille that only the four-methyl face can generate the α-to-α and α-to-γ epitaxial growth.[18] Furthermore, helices can deposit in two different ways: continuous α-phase growth with antichiral parallel stem orientations along the *b*-axis or epitaxial growth with different stem orientations. Figure 2 shows the two possible ways of stem deposition on the four-methyl growth face parallel to the *ac*-plane.[30] As shown in Figure 2a, when the deposited antichiral stem orientation along the *b*-axis is identical to those at the four-methyl face, the continuous α-phase growth can be observed (the a_1 and a_2 and the c_1 and c_2 are parallel to each other in Figure 2a). However, Figure 2b illustrates that two isochiral helical stems can also orient at the 80° or 100° tilt between them because the *a*- and *c*-axis dimensions of the α-phase unit cell are very close to each other, and the crystal lattice matches well when the stem tilts 80° or 100°. After this molecular epitaxy, if the subsequent stems permanently keep this changed stem orientation with antichiral packing of the stem helices, it will lead to epitaxy between the two α-phases. This is the α-to-α phase lamellar branching, also known as cross-hatching, which is carried out by an α-phase lamella growing on its mother α-phase lamella with its *a*- and *c*-axes in the real lattice (the a_1 and c_1 in Figure 2b) oriented with the *c*- and *a*-axes (the c_3 and a_3 in Figure 2b) of the mother lamella, respectively.[29−33]

On the other hand, there is another type of molecular epitaxy: the growth of the γ-phase on the α-phase. The origin of the epitaxial conversion between the α-phase and the γ-phase has been correctly reported in the case of low MW i-PP samples.[13,14] The new γ-phase requires an alternation of the stems in each of the two layers by changing their orientation between the *a*- and *c*-axes

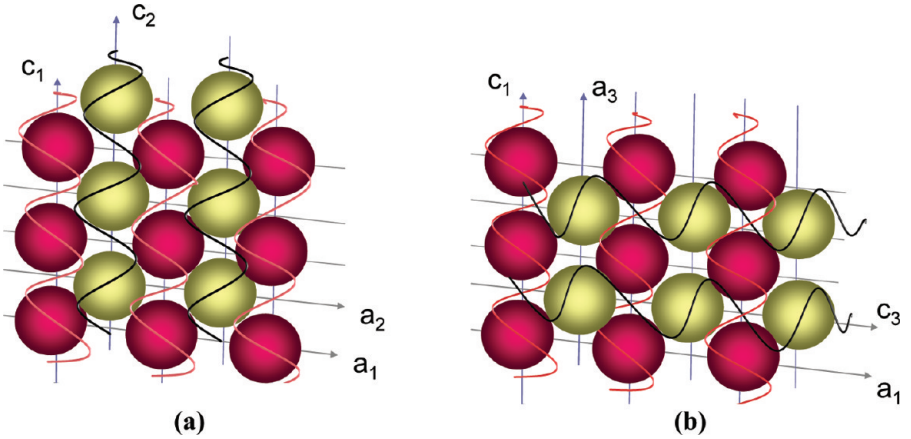

Figure 2. (a) Illustration of parallel deposition of the i-PP helices on the *ac*-plane of the α-phase giving rise to a continuous α-phase growth. The methyl groups at the growth face are marked by red circles within the a_1c_1-plane. The methyl groups which are marked by yellow circles represent the depositing antichiral stem in the a_2c_2-plane which are parallel to the stem orientation in the original α-phase crystal (a_1 is parallel to a_2, and c_1 is parallel to c_2). (b) Molecular epitaxial deposition of the i-PP helices on the *ac*-plane of the α-phase leading to the lamellar branching (the cross-hatching) or the γ-phase in i-PP. The methyl groups at the growth face are marked by red circles within the a_1c_1-plane. The methyl groups which are marked by yellow circles represent the depositing stem with the a_3c_3-plane which is either 80° or 100° away from the stem orientation in the original α-phase crystal (reprinted from ref 30 with permission).

of the α-phase lattice. In relation to the original α-phase, this is the α-to-γ molecular branching. In principle, it is also possible to observe the epitaxial conversion of the γ-phase back to the α-phase, or in a more general case, multiple reversible epitaxial conversions between the α-phase and the γ-phase should occur.

In this publication, using specifically synthesized high MW i-PP samples containing different amounts of stereodefects, we are able to observe two apparently different types of morphology of the γ-phase: needle-like crystals and "flat" lamellae, which are determined by the stem orientation of the initial elongated α-phase single crystals. Furthermore, formation mechanisms of these morphologies of the γ-phase crystals are also discussed.

Experimental Section

Materials and Samples. The three stereodefective i-PP fractions used in this study were prepared with a highly regiospecific metallocene catalyst that is described in refs 22 and 23. It has been reported that this set of samples provided a majority of the γ-phase during crystallization under a crystallization temperature region between 100 and 140 °C at atmospheric pressure. The MW, melting temperatures, main microstructural characteristics, polydispersity index of the molecular masses, polymerization temperature, and the catalytic system used for synthesis of the samples (designated as R1, R2, and R3) are described in Table 1. These three samples showed basically identical phase behaviors and crystal morphologies, and therefore, no specific identification of the samples was needed for this report.

Thin films were prepared for TEM and AFM experiments by a solution-casting method. The solution was prepared by dissolving the samples into octane with a concentration of 0.005% (w/v) at 110 °C. The solution was then dropped onto carbon-coated mica surfaces that had been freshly cleaved. The solvent was evaporated at room temperature in vacuum. It was found that the thin films, after this drying process, did not completely cover the mica surface. In the area where the i-PP films were found, the thickness was around 16 nm. In other areas, the bare carbon-coated mica surface was observed without the i-PP sample. The samples were then heated to 180 °C and held there isothermally for 5 min in a hot stage (Mettler FP90) before they were quickly transferred to another hot stage (Mettler FP90) which was preset at an isothermal crystallization temperature (T_x) of 120 °C for a prolonged time (about 48−72 h). All the isothermal crystallization processes were conducted in a dry nitrogen atmosphere. The thin films were then separated from the mica surface by floating the samples on distilled water and were picked up on copper grids for analysis.

Instrumentation and Experiments. Observation of the overall crystal morphology was first performed under phase contrast light microscopy. Bright field (BF) and dark field (DF) images of the crystal morphologies were observed with a transmission electron microscope (TEM, Philips Tecnai) at an accelerating voltage of 120 kV. Selected area electron diffraction (SAED) experiments with a rotating/tilting stage were also conducted in the TEM. In order to achieve ED patterns with different crystal orientations, a tilting stage was attached to the sample holder. The tilting angle was defined as positive if the tilting direction was clockwise and negative for counter-clockwise. The dark field (DF) technique was utilized by centering the inserted objective aperture and tilting the beam so that the chosen diffraction spot in the diffraction pattern would go through the objective aperture. The advantage of DF imaging obtained in this way is its inherently high and diffraction-selective contrast. In order to limit electron beam damage, the grid was initially scanned by defocusing the beam in the diffraction mode at low magnification. To investigate crystal morphologies, the i-PP thin films were sometimes shadowed with Pt at an angle of 30° to increase the image contrast. BF images of these samples after platinum coating were then taken by TEM. Molecular modeling and analysis of the diffraction patterns were performed using the Cerius^2 package of Accelrys.

Table 1. Characteristics of the Three Stereodefective i-PP Samples (R1, R2, R3), a *rac*-Isopropylidene[bis(3-trimethylsilyl)(indenyl)]-zirconium/MAO Catalytic System[22,23]

samples	molecular weight (M_w)	T_m (°C)	[mmmm] (%)	[rr] (%)	polydispersity	T_{polym} (°C)
R1	110 000	144	89.0	2.3	2	20
R2	75 000	141	87.4	2.6	2	50
R3	66 000	137	83.4	3.4	2	60

AFM (Digital Instrument Nanoscope IIIA) was used to examine the surface of the i-PP crystals grown at T_x = 120 °C for 72 h from the thin film melt on the mica substrates. A 100 μm scanner was selected, and the tapping mode was used to obtain both the height and phase image. The cantilever force was light enough to limit damage to the sample, yet strong enough so that the surface features could be accurately explored. The scanning rate was 1−3 Hz for low-magnification images at a resolution of 512 × 512 pixels per image.

Results and Discussion

Needle-Like Morphology of the γ-Phase Crystals. Figure 3a shows a TEM BF image of the typical crystal morphology observed in this series of stereodefective i-PP samples crystallized at T_x = 120 °C for 72 h from the thin film melt. This image exhibits an elongated single crystal at the center and needle-like crystal overgrowth along both edges of the single crystal (the circles in this figure are the areas where the SAED patterns were taken and will be discussed below with Figure 5). Figure 3b shows an AFM image of the same i-PP crystal morphology under the identical crystallization conditions as shown in Figure 3a. This needle-like crystal morphology here observed is similar to the observations by Geil in the 1960s (Figures III-30 and III-31 in ref 34), yet the ED experiment was not conducted at that time, and thus, no crystal structure identifications were made (see below). The image of Figure 3b also includes a height scan which was taken separately along the long axis (Figure 3c) and the transverse axis (parts d−f of Figure 3) of the initial elongated single crystal. By scanning along the elongated axis of the initial single crystal, we obtain the average thickness of needle-like crystals which is about 15 nm compared with the bare carbon-coated mica surface (Figure 3c). It seems that the needle-like crystals possess larger widths near the initial elongated single crystal and taper off continuously by decreasing the width toward the growth tips. At the tip of the needle-like crystal, its width and thickness are almost identical. By scanning the transverse axis of this single crystal, we obtain a thickness of the initial elongated single crystal of about 13 nm in a region without the needle-like crystals (Figure 3e), and its width along the transverse direction is about 120 nm (Figure 3f).

Figure 4a shows a BF image which exhibits needle-like crystal morphology after the sample was shadowed with platinum. It is evident that these needle-like crystals are often 2D bundles, yet their individual width is close to constant at around 15 nm. At distances further from the initial elongated single crystal, the number of these needle-like crystals in the 2D bundle decreases, and the bundles become narrower. The effect of platinum shadowing in the TEM experiments compared with the noncoated sample as shown in Figure 3a clearly shows the individual needle-like crystals where they could not be distinguished previously.

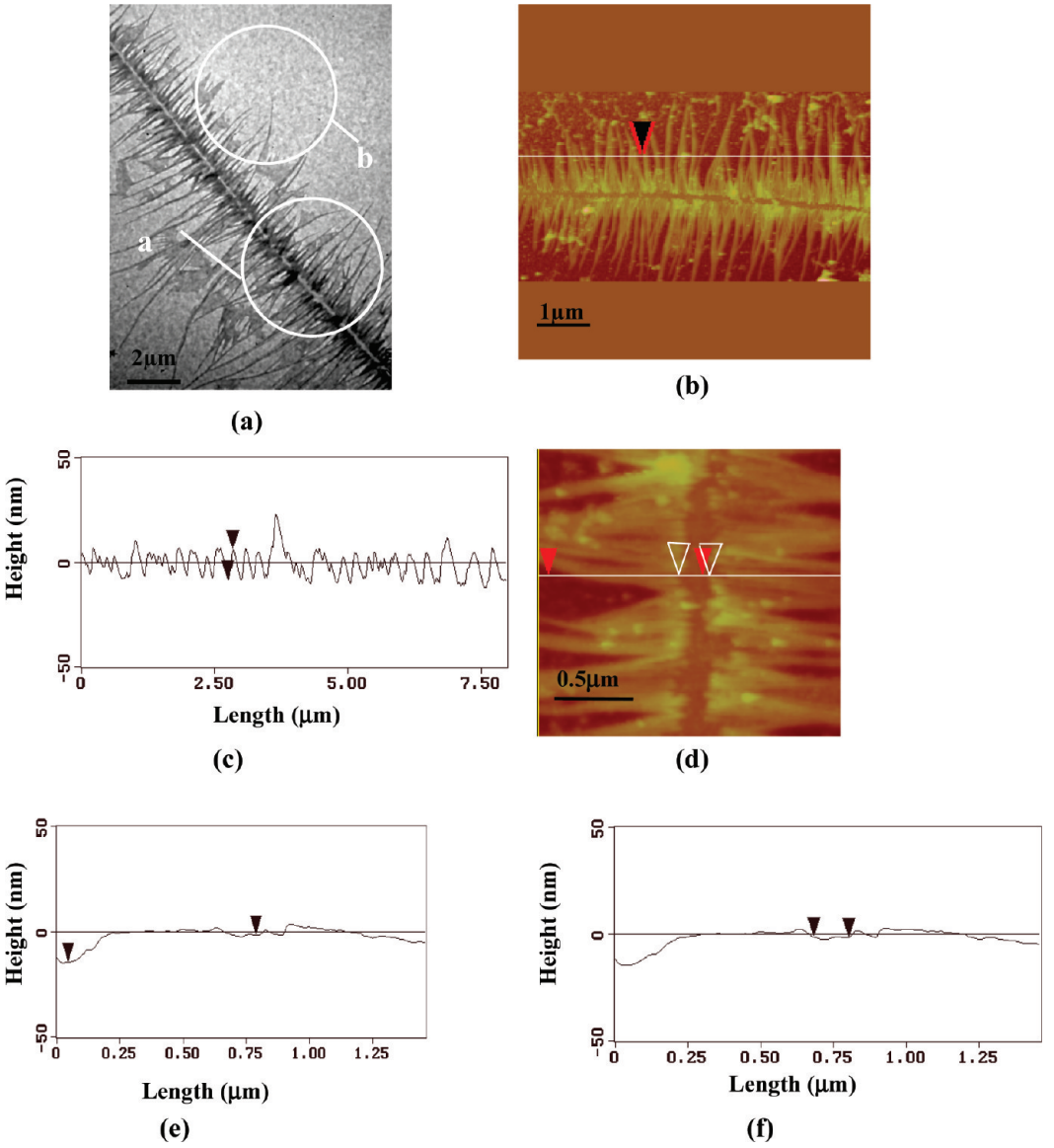

Figure 3. (a) BF image of stereodefective i-PP crystal morphology isothermally crystallized from the thin film melt at T_x = 120 °C for 72 h. The elongated single crystal is at the center, and the needle-like crystals are overgrowths along the two edges of the single crystal. (b) AFM image of crystal morphology in an i-PP thin film grown at the identical conditions. The morphology was observed at room temperature. (c) A height scan of the above crystal along the elongated axis (the scanning direction and position are shown in part b). The difference between the two arrows represents the height of the needle-like crystal. The peak in the middle of the scan may be associated with dust. (d) Another AFM image of the crystal morphology in an i-PP thin film grown at identical conditions. (e) A height scan of the crystal in (d) along the transverse axis with scanning direction and position as shown in part d. The difference of the two arrows represents the height of the elongated single crystal at the center part of this morphology. (f) The width of the same elongated single crystal at the center part of this morphology shown in part d along the transverse axis. The distance between the two arrows represents the size of the elongated single crystal along this scanning direction.

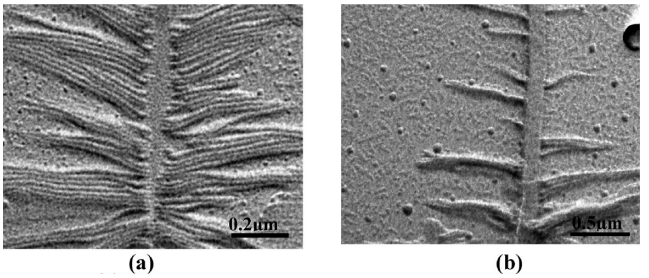

Figure 4. BF images of needle-like crystal morphology isothermally crystallized from the thin film melt at T_x = 120 °C for different times after platinum coating: (a) after fully developed needle-like crystals and (b) development of these crystals in the areas without sufficient i-PP sample.

Figure 4b shows a growth of these needle-like crystals where the i-PP has much less coverage on the mica surface (thus less sample was available during the crystallization) and when crystallized for a shorter time. Indeed, they begin to grow individually by epitaxy on the initial elongated single crystal.

In order to determine whether the initial elongated single crystal and the needle-like crystals belong to the same crystal structure, SAED experiments were carried out. Figure 5a is an SAED pattern obtained from the crystal morphology in Figure 3a (circle a), and the pattern is oriented in the correct direction with the crystals in Figure 3a. It is speculated that this ED pattern is a mixed pattern attributed to both the α-phase and the γ-phase lattices with two different zones. Generally speaking, the α-phase is characterized by

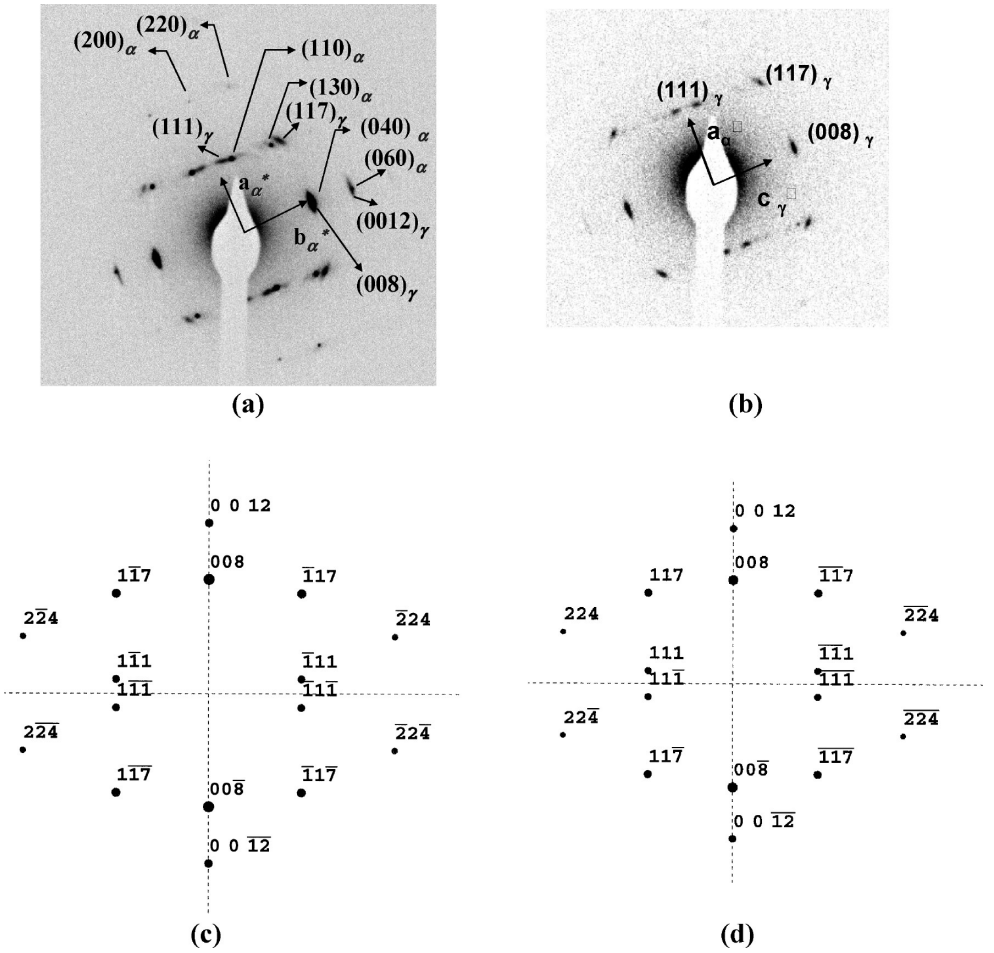

Figure 5. (a) SAED patterns of needle-like i-PP γ-phase crystals in Figure 3 (circle a). The SAED pattern is in the correct orientation with respect to the crystal morphology shown. (b) SAED pattern obtained which is solely attributed to the needle-like crystals (from the γ-phase of the i-PP sample in circle b). (c) [110] zone ED pattern of the γ-phase calculated based on the Cerius[2] crystallographic modeling package. (d) [$\bar{1}$10] zone ED pattern of the γ-phase calculated with the help of the Cerius[2] crystallographic modeling package.

relatively sharp diffraction spots, while the γ-phases are relatively wide diffraction arcs. In this ED pattern, the diffractions of the α-phase must be obtained from the initial elongated single crystal, and the γ-phase pattern is attributed to many needle-like crystals with a relatively uniform orientation. The next step is to confirm this assumption through crystallographic analysis.

Detailed crystallographic analysis of Figure 5a indicates that the a^*-axis of the α-phase was parallel to the elongated direction of the initial single crystal, and the b-axis was parallel to the transverse axes of the initial single crystal. The α-phase diffraction spots can be indexed as the (040), (060), (110), (130), (200), and (220) planes as assigned in this figure. The stem orientation is along the c-axis and is parallel to the thin film (lamellae) normal; therefore, Figure 5a is, in part, the [00l] zone ED pattern of the α-phase crystal.

Figure 5b shows an SAED pattern which was taken only in the area of the needle-like crystals in Figure 3a (circle b). Compared to the [110] or [$\bar{1}$10] zone ED pattern of the γ-phase unit cell obtained from the Cerius[2] package as shown in parts c and d of Figure 5, respectively, the diffraction arcs in Figure 5b must belong to the γ-phase crystals, and they can be indexed as the (008), (0012), ($\bar{1}$11), ($\bar{1}$17) planes from the [110] zone or the (008), (0012), (111), (117) from the [$\bar{1}$10] zone. The needle-like crystals are thus the γ-phase with an orientation of the needle direction (the growth direction) along the c-axis. The cross-section of this needle-like crystal is the ab-plane. The stems in the needle-like γ-phase crystals have two orientation directions (80° or 100° apart from each other) which are parallel to the two different corresponding diagonals of the ab-plane. Therefore, the resulting diffraction patterns along these two stem directions in the needle-like γ-phase crystals correspond to the [110] zone shown in Figure 5c or the [$\bar{1}$10] zone shown in Figure 5d, and they are crystallographically equivalent.

The Cerius[2] simulation confirms that the diffraction arcs in Figure 5a belong to the γ-phase diffractions with either the [110] or the [$\bar{1}$10] zone. This ED pattern thus possesses the mixed diffraction patterns of both the α- and γ-phases. If we subtract all the diffraction arcs which are attributed to the γ-phase, the remaining diffraction pattern is the pure α-phase ED pattern from the [00l] zone.

Formation Mechanism of the Needle-Like γ-Phase Crystal. The question that arises is: why do the γ-phase crystals adopt the needle-like morphology? The answer must be associated with the stem orientations within the γ-phase crystals that are epitaxially grown on the α-phase crystals in these high MW i-PP samples. It is known that the stem orientation in the γ-phase alternates 80° (or −80°) in every two stem layers along the c-axis. Note that the initial elongated α-phase single crystal is "flat-on" with its stem orientation parallel to the thin film normal. The first layer of the stems to initiate the γ-phase has to be epitaxially oriented 80° (or −80°) away from this stem orientation of the α-phase single crystal. However, after two antichiral helical stem layers are oriented in this way, the stems in the third layer along the c-axis switch

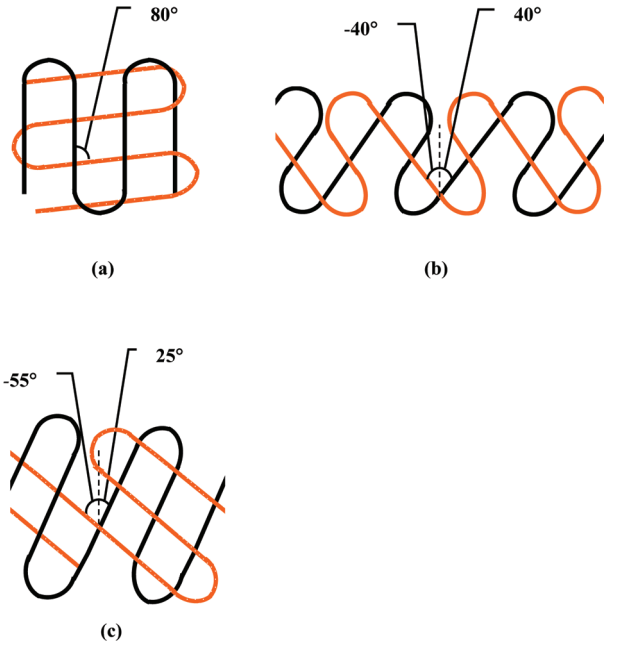

Figure 6. Schematic illustrations of 2D projections of three growth modes of the γ-phase crystals in i-PP which possess different stem orientations with respect to the thin film normal. The black stems are in the outermost stem layer of the α-phase crystal, and the orange stems are the first layer of the molecular epitaxy growth of the γ-phase crystal. (a) Stem packing model of the needle-like γ-phase crystal. (b) ±40° stem packing model of the "flat" γ-phase lamellar crystal. (c) 25°-tilted stem packing model of the α-phase and the γ-phase of the "flat" γ-phase lamellar crystal.

back (parallel to the thin film normal), again by the molecular epitaxial growth. The stems in the growth face of the second layer and the molecular epitaxially deposited stems of the third layer are isochiral. This alternating orientation changes every two stem layers leading to the formation of the γ-phase crystal.

Figure 6a illustrates a schematic 2D projection of the first layer of such molecular epitaxy growth of the stems in a γ-phase crystal (orange stems) on the outermost stem layer of the *ac*-plane of the α-phase crystal (black stems). The *c*-axis of the γ-phase crystal is along the needle direction. Assuming that the chain folding of the initial elongated α-phase single crystal is within the *ac*-plane, the needle-like γ-phase is within the *ab*-plane (note that these two planes are parallel to each other). Furthermore, there are two stem orientation directions within the *ab*-plane of the γ-phase which are 80° or −80° apart from each other. In this needle-like γ-phase crystal, therefore, both of the lateral surfaces in the *ab*-plane contain chain folds, and the fold planes are close to the (340) and $(3\bar{4}0)$ planes.

The γ-phase epitaxy growth in this model (Figure 6a) must be limited by the thickness of the α-phase single crystal that was 13 nm. This thickness provides the upper-limit of the thickness of the epitaxial growth of the γ-phase crystal on the surface of the α-phase crystal along the thin film normal. Further growth would evoke that the lateral size of the γ-phase crystal exceeds this thickness and leads to a creation of new surface free energies. However, the stem orientation of this first layer is ±80° with respect to the thin film normal and it is thus ±10° away from the direction parallel to the thin film. Therefore, the stem length along this direction should not be affected by the stem thickness of the α-phase single crystal. The question is whether the first stem layer of the needle-like γ-phase crystals epitaxially grown on the *ac*-plane of the α-phase single crystal may increase its stem

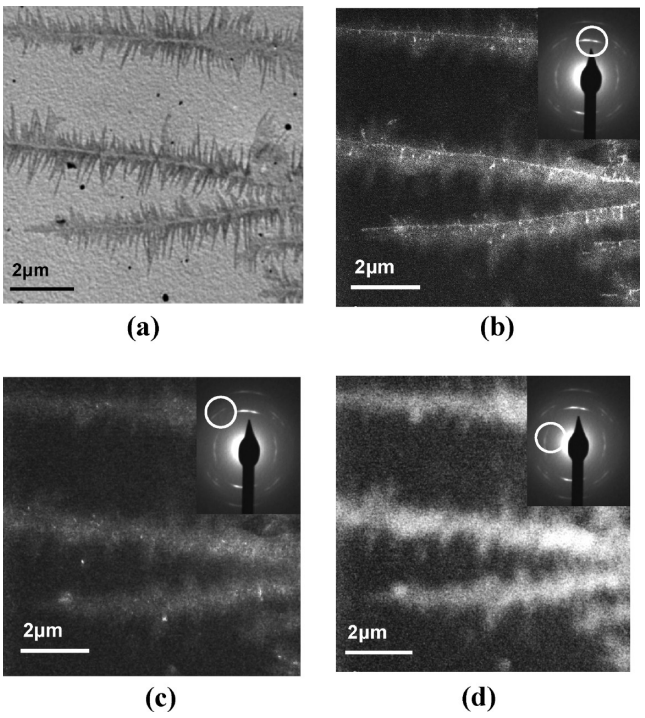

Figure 7. (a) BF image of the i-PP sample with needle-like γ-phase crystals isothermally crystallized at T_x = 120 °C for 72 h from the thin film melt. Set of DF images of (b) $(008)_\gamma$ and $(040)_\alpha$, (c) the $(117)_\gamma$, and (d) the $(111)_\gamma$ and $(11\bar{1})_\gamma$. The ED patterns are also inserted with correct orientation to illustrate the generation of the DF images.

length to further stabilize the crystal. Our morphological observation indicates that the stem length of the needle-like γ-phase crystals along both directions prefer to keep a constant value of about 15 nm. This is due to the fact that the stem length of this γ-phase along the direction that is ±80° away from the direction of the thin film normal has to be determined based on the growth principle that the length must be proportional to the reciprocal supercooling.[35] After the first stem layer of the γ-phase crystal grows with the fixed size, the molecular epitaxial growth during subsequent development of the needle-like γ-phase crystals are self-constrained by the previously deposited stem lengths along both directions.

It was speculated that any crystal growth above the thin film thickness may also feel the film confinement due to the difficulty of transporting the chains on the crystal growth surface. We have conducted experiments with different thin film thickness ranging from 16 to 40 nm. The identical morphology and size of needle-like γ-phase crystals were observed. Therefore, the thin film thickness must have no effect on the formation of needle-like crystals in this film thickness range. In Figure 6a, the needle growth direction is along the *c*-axis of the γ-phase that is perpendicular to the figure, yet both the lateral sizes of the needle-like crystals are similar to the lamellar thickness of the "flat-on" α-phase single crystal.

One BF and three DF images of needle-like γ-phase crystals are shown in parts a−d of Figure 7. In the BF image (Figure 7a), we observe five initial elongated α-phase crystals (large and small) with epitaxially grown needle-like γ-phase crystals which are more or less parallel to each other. Based on the structural analysis described above, the α-phase single crystals are "flat-on," and the overgrown needle-like crystals are the γ-phase. Figure 7b shows a DF image using both the $(040)_\alpha$ ED spot and the $(008)_\gamma$ ED arc. The bright streaks in Figure 7b appear because in these areas the $(040)_\alpha$ planes are

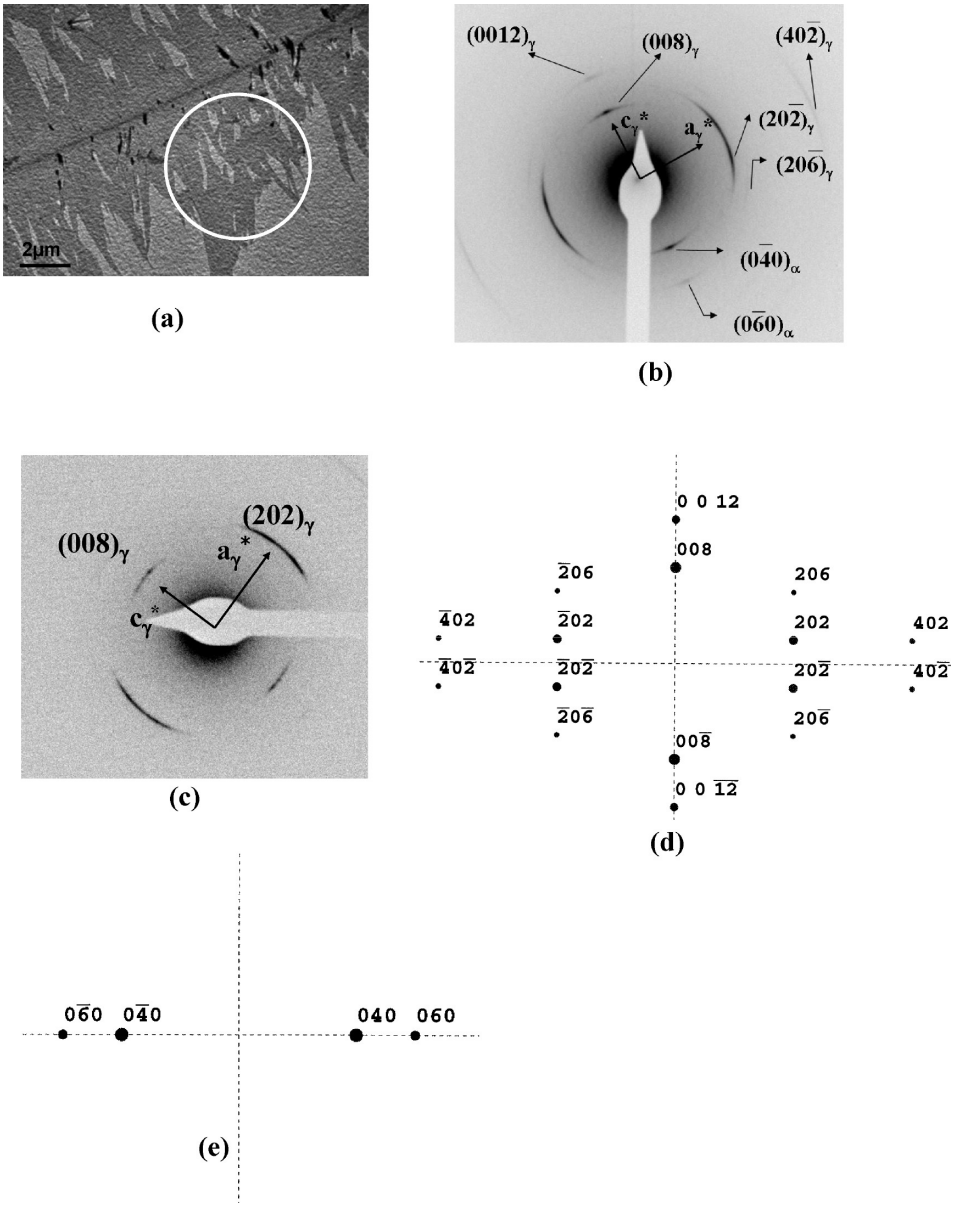

Figure 8. (a) BF image of the i-PP sample with γ-phase crystals isothermally crystallized at T_x = 120 °C for 72 h from the thin film melt. (b) ED pattern without inserting a selected-area aperture obtained from part a, and thus, both the elongated α-phase crystal and "flat" γ-phase lamellar crystal are included. (c) ED pattern after inserting a selected-area aperture obtained from part a specifically focusing on the "flat" γ-phase lamellar crystal. (d) ED pattern of the γ-phase crystal from the [010] zone using the Cerius^2 crystallographic modeling package. (e) Calculated ED pattern of the α-phase from the [205] zone.

parallel to the thin film normal. Meanwhile, in the less bright areas of the γ-phase crystals, the [110] zone axis orientation of the needle-like γ-phase crystals may slightly deviate from the condition that the $(008)_\gamma$ planes are perfectly parallel to the thin film normal due, possibly, to slight twisting during the growth along the *c*-axis of the γ-phase. Parts c and d of Figure 7c are the $(117)_\gamma$ and the $(111)_\gamma$ and $(11\bar{1})_\gamma$ DF images of the needle-like γ-phase crystals. In both figures, each needle-like γ-phase crystal shows a gradual decrease in intensity along the *c*-axis away from the initial elongated α-phase crystal. This might be explained by the [110] zone axis orientation of γ-phase crystals gradually deviating as they grow further away from the α-phase crystals due to a lamellar twist. Both the $(117)_\gamma$ and the $(111)_\gamma$ and $(11\bar{1})_\gamma$ DF images show no bright streaks attributed to the initial elongated α-phase single crystal.

The "Flat" γ-Phase Single Crystals. One would assume that the needle-like morphology is not the stereodefective i-PP γ-phase with the lowest free energy state since the crystal metastability is determined by the crystal size.[35] Figure 8a is a TEM BF image that illustrates that "flat" lamellar crystals can also be observed as overgrowth on the initial elongated α-phase crystal. If these overgrown crystals are γ-phase lamellar crystals, the question arises as to how this flat γ-phase lamellar crystal develops epitaxially.

An answer can be postulated that the stem orientation of the initial α-phase single crystal is not parallel to the thin film normal, but tilted within the *ac*-plane at an angle θ (not parallel to the thin film normal). Since the first layer of stems to initiate the γ-phase has to be epitaxially oriented ±80° (or less possible, ±100°) away from this initial stem orientation in the α-phase single crystal, we can then have the stems in this layer tilted in the opposite direction of the *ac*-plane by 80°−θ with respect to the thin film normal. If θ = 40°, the epitaxial crystal growth mode is shown in Figure 6b as a schematic illustration of a 2D projection of

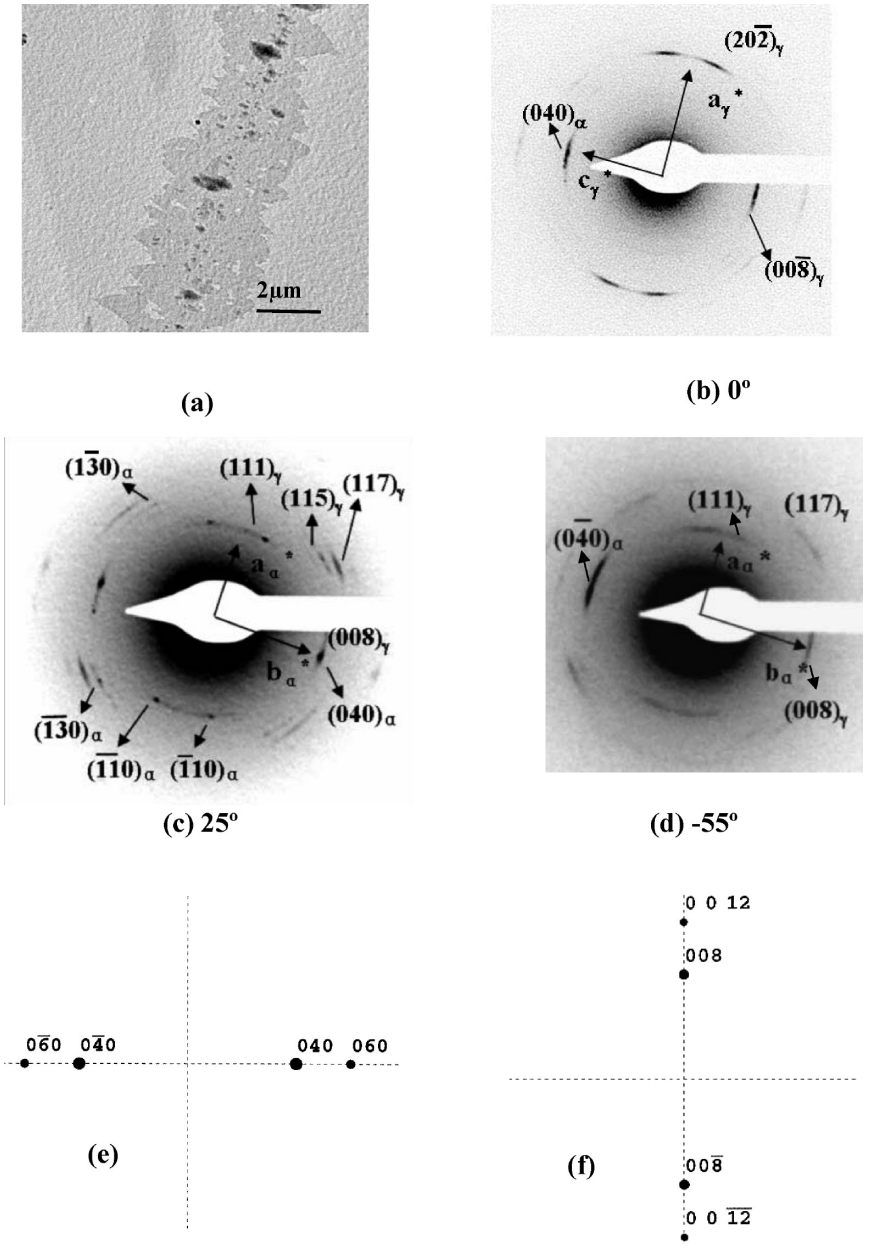

Figure 9. (a) BF image of the γ-phase lamellar crystal morphology for the i-PP sample isothermally crystallized at T_x = 120 °C for 72 h from the thin film melt. (b) SAED pattern of (a) without tilting. (c) SAED after tilting 25° away from the thin film normal around the *b*-axis of the initial elongated α-phase crystal. (d) SAED after tilting −55° away from the thin film normal around the *b*-axis of the initial elongated α-phase crystal. (e) Calculated ED pattern of the α-phase from the [205] zone. (f) Calculated ED pattern of the γ-phase from the [130] (or [$\bar{1}$30]) zone.

two stem layers with one as the outermost layer of the *ac*-plane of the initial elongated α-phase single crystals (black stems) and another the first layer of the γ-phase crystals epitaxially grown on the α-phase crystals (orange stems) on top of the outermost black stem layer. The γ-phase can thus have two stem orientation directions in the crystal: both are tilted either at ±40° with respect to the film normal within the *ab*-plane of the γ-phase. Again, the growth direction along the *c*-axis is perpendicular to this figure. This should lead to a growth of the "flat" γ-phase single crystal.

In order to verify this postulation, ED experiments were carried out. Figure 8b is an ED pattern taken from the overall crystals shown in Figure 8a (without selective area). It is evident that Figure 8b is also a mixed ED pattern containing both the γ- and α-phases. If we use the SAED technique to only focus on the γ-phase lamellar crystal (the circle in Figure 8a), we obtain an ED pattern as shown in Figure 8c. It is a pure γ-phase ED from the [010] zone. This indicates that the stems in this γ-phase lamellar crystal do possess a ±40° orientation with respect to the thin film normal. Utilizing the Cerius[2] crystallographic package, we can construct ED patterns of the γ-phase from the [010] zone as shown in Figure 8d. After subtracting the γ-phase spots from Figure 8b, as shown in Figure 8c, the remaining ED pattern is only attributed to the α-phase. The simulated pattern by the Cerius[2] crystallographic package is shown in Figure 8e. In Figure 8b, only the α-phase spots which resulted from the (0*k*0) planes are observed, and all the spots produced by the original (1*k*0) planes which are found in the ED pattern of the "flat-on" α-phase single crystal from the [001] zone are not observed. Therefore, it can be concluded that the stems of the α-phase crystal are tilted at some angle θ within the *ac*-plane around the *b*-axis.

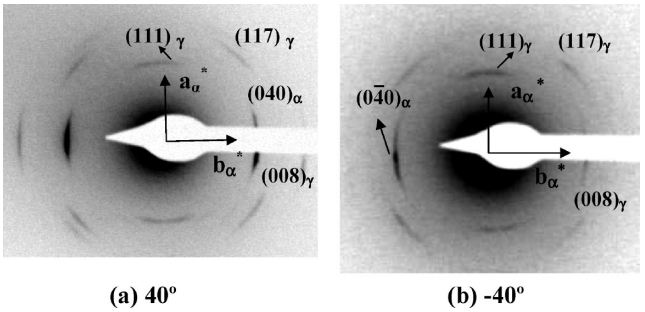

Figure 10. (a) SAED of γ-phase lamellar crystal after tilting 40° away from the thin film normal within the *ac*-plane of the initial elongated α-phase crystal for the i-PP sample as shown in Figure 9a. (b) SAED after tilting −40° away from the thin film normal around the *b*-axis of the initial elongated α-phase crystal.

We have found no report that the stem orientation of the α-phase single crystal in i-PP has deviated from the thin film normal with a large angle. Furthermore, can we identify that this nonparallel stem orientation with respect to the thin film normal is $\theta = 40°$? This question can be answered by utilizing tilted SAED experiments on the samples. We can precisely determine the θ-angle of the stems of the α-phase with respect to the thin film normal within the *ac*-plane by tilting the initial elongated α-phase crystal around the *b*-axis until the ED pattern from the [00*l*] zone of the α-phase appears. Furthermore, we can examine the epitaxial relationship of this phase with the α-phase from the ED pattern of the γ-phase at that tilting angle.

Figure 9a is the morphology of the "flat" γ-phase crystal with an initial elongated α-phase crystal. When we take an ED for both crystals, Figure 9b is identical to Figure 8b with a different orientation. If we tilt the crystal around the *b*-axis of the α-phase at different angles, we find the [001] zone of the α-phase after the tilting angle reaches 25° as shown in Figure 9c. In this figure, we also observe a γ-phase ED pattern with the [110] or [$\bar{1}$10] zone, and this pattern can also be observed when we tilt the "flat" γ-phase crystal −55° away from the thin film normal as shown in Figure 9d. Calculations indicate that the 25°-tilted (or −25°-tilted) α-phase stems in the *ac*-plane exhibit the [205] zone as shown in Figure 9e, while the −55°-tilted (or 55°-tilted) γ-phase crystal generates the γ-phase ED pattern from the [$\bar{1}$30] (or the [130]) zone. This reveals, as shown in Figure 9f, that the 80° molecular epitaxial growth between the α-phase and the γ-phase crystals is still maintained for this sample. The folded surface in this case is close to the (140) plane. A 2D projection of two interfacial stem layers is shown in Figure 6c. In this figure, the outermost layer of the *ac*-plane of the initial elongated α-phase single crystal (black stems) is tilted 25° away from the thin film normal. The first layer of the γ-phase crystal epitaxially grown on the α-phase crystal (orange stems) on top of the outermost black stem layer, on the other hand, is tilted −55° away from the thin film normal within the *ab*-plane of the γ-phase lamellar crystal.

However, when we take ED patterns of the crystal in Figure 9a by tilting the crystal ± 40° away from the thin film normal within the *ac*-plane of the initial elongated α-phase crystal, the ED patterns of the "flat" γ-phase crystal with the [110] and [$\bar{1}$10] zones can also be obtained as shown in parts a and b of Figure 10. In this case, the folded surface is close to the (010) plane. Therefore, it is speculated that from the initial growth of the 25°-tilted γ-phase crystals, the γ-phase crystals continuously twist their stem orientation along the *c*-axis until the ± 40° titled "flat" γ-phase lamellar crystals are reached.

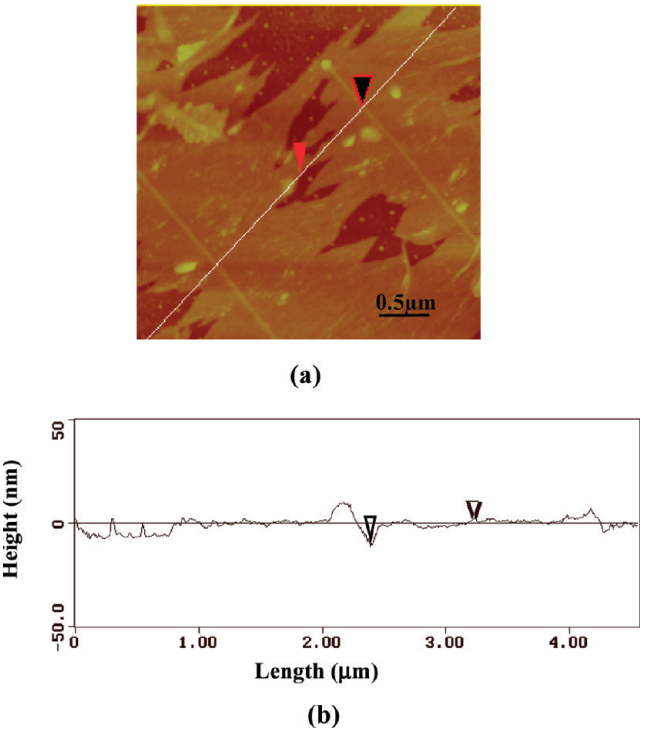

Figure 11. (a) AFM image of the γ-phase lamellar crystal morphology for the i-PP sample isothermally crystallized at T_x = 120 °C for 72 h from the thin film melt. (b) Height scan along the transverse direction of the α-phase crystal (the *b*-axis). The scanning direction and position are shown in part a. The difference between the two arrows represents the "flat" lamellar thickness of the γ-phase.

Figure 11a shows an AFM image of "flat" γ-phase lamellar crystals of the i-PP sample isothermally crystallized from the thin film melt under identical conditions. In this figure, there are two initial elongated α-phase crystals. Both of them initiate the "flat" γ-phase lamellar crystals. Figure 11b is a height scan taken along the direction perpendicular to the initial elongated α-phase crystal. The scanning direction and position of this figure are also shown in Figure 11a. The thickness of the elongated α-phase crystal is about 14 nm, and the transverse width of the α-phase crystals is about 60 nm. On the other hand, the thickness of the overgrown "flat" γ-phase lamellar crystals is around 12 nm. Note that the stems are tilted at an angle of 40°; therefore, the stem lengths in the crystal should be longer than 12 nm. There were possibly two different stem lengths that existed in the initially grown γ-phase as shown in Figure 6c.

In order to further demonstrate the stem orientation in the "flat" γ-phase lamellar crystals, DF experiments were also carried out. Figure 12a is a BF image of a "flat" γ-phase lamellar crystal. Figure 12b is a DF image of this crystal generated using both the $(040)_\alpha$ ED spot and the $(008)_\gamma$ ED arc. We observe several bright lines more or less parallel to each other. These bright lines are generated under the condition that the $(040)_\alpha$ planes of the elongated α-phase crystals are parallel to the direction of electron beam. Furthermore, we can also observe that the less bright area of the "flat" γ-phase lamellae are generated under the condition that the $(008)_\gamma$ planes of these crystals are parallel to the direction of the electron beam. Here, because the electron density of the $(040)_\alpha$ planes is higher than the $(008)_\gamma$ planes, the "flat" γ-phase lamellae are less bright than the elongated α-phase single crystal. Figure 12c shows a $(202)_\gamma$ and $(20\bar{2})_\gamma$ DF image of the "flat" γ-phase crystals. In

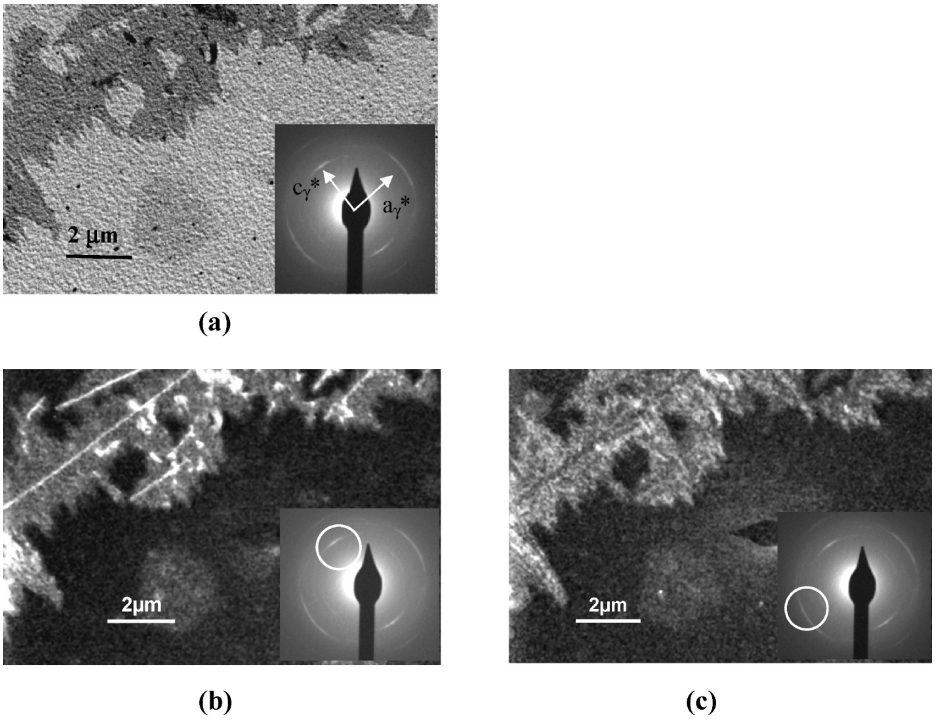

Figure 12. (a) BF image, (b) $(008)_\gamma$ and $(040)_\alpha$ DF image, and (c) $(202)_\gamma$ and $(20\bar{2})_\gamma$ dark field image of the i-PP sample with "flat" γ-phase crystals isothermally crystallized at T_x = 120 °C for 72 h from the thin film melt. Three ED patterns are also inserted in parts a, b, and c with the correct orientations. The dark areas in part a are caused by overgrowth of the α-phase crystals. This can be proven by the DF observation in part b since all of these areas are brighter than the areas of the "flat" γ-phase crystals.

this figure, bright lamellar crystals are attributed to the γ-phase, while the elongated α-phase single crystal has no contribution. Note that the "flat" γ-phase crystals in this case exhibit the [010] zone, and the *b*-axis orientation in the "flat" γ-phase crystals is parallel to the direction of electron beam. Thus, the $(202)_\gamma$ and $(20\bar{2})_\gamma$ planes are the only contributors to generate the bright areas in Figure 12c.

What Issues Remain? The formation of the "flat" γ-phase lamellar crystals initiates from the epitaxial growth of the 25°-tilted stem orientation along the *ac*-plane of the elongated α-phase single crystal. There are two possibilities for the cause of this tilting. First, the tilted stem orientation of the elongated α-phase crystal is initially parallel to the thin film normal and becomes tilted after growth of the γ-phase. With an increasing number of epitaxially grown needle-like γ-phase crystals, these needle-like crystals have a tendency to twist and accommodate the growth of the more stable "flat" γ-phase lamellar crystals. This cooperative twist may force the tilt of the stem orientation in the elongated α-phase single crystal along the *ac*-plane. If this possibility is true, we should then observe a continuous tilting of the stems of the elongated α-phase crystals. We may then observe the ED pattern of α-phase crystals with the [00*l*] zone at different tilting angles around the *b*-axis. Moreover, an equally important question would be why the initial tilting angle is only 25°.

The second possibility is that, intrinsically, the elongated α-phase single crystals possess the tilted stem orientation within the *ac*-plane. To confirm this, it requires that we grow elongated α-phase single crystals without overgrowth of the γ-phase crystals. In this case, it is impossible for the γ-phase overgrowth to generate the torque from the cooperative twist. ED experiments can then be carried out on these single crystals to determine whether the stem orientation in these elongated α-phase crystals is tilted within the *ac*-plane.

Another outstanding issue is how the chain folds in the γ-phase crystals. Polyethylene (PE) decoration may provide a straight answer. [36−38] However, the methyl groups on the i-PP chains in the crystal lattice may obscure the decorated PE rod crystals when these groups are at the top of the lamellar folded surfaces. A very light decoration of PE may be necessary. All of these issues are currently undergoing investigation and results will be reported in a future publication.

Conclusion

In summary, detailed structural and morphological analyses performed based on our TEM, AFM, and SAED experiments indicate that in these i-PP samples, all of the γ-phase crystals were grown epitaxially on an initial elongated α-phase single crystal, as correctly pointed out by several previous research groups. When the initial α-phase single crystal possesses a stem orientation that is parallel to the thin film normal (the crystal ED pattern possesses the [00*l*] zone), the epitaxially grown γ-phase on the *ac*-plane of the initial α-phase single crystal forms the needle-like crystals with the needle direction along the *c*-axis of the γ-phase unit cell. The reason for this needle-like crystal formation is that the epitaxial growth of the γ-phase crystal is limited by both the lamellar thickness of the α-phase "flat-on" elongated crystal in the direction parallel to the thin film normal and the growth principle that the length must be proportional to the reciprocal supercooling in the direction of ±80° away from this normal.

The second γ-phase crystalline morphology is a "flat" lamella. This requires that the initial α-phase single crystal has a stem orientation tilted away from the thin film normal around the *b*-axis within the *ac*-plane. Tilted ED experimental results have shown the stem of the initial α-phase single crystal was tilted up to 25° away from the thin film normal, and at the tilted angle of 25°, the ED pattern exhibits the [205] zone. Therefore, the morphological conversion from the needle-like to the "flat"

γ-phase crystals was the change of the stem orientation direction of the initial α-phase single crystals. Furthermore, the final "flat" γ-phase lamellar crystals with the stem orientations of ±40° from the thin film normal were developed by a possible continuous twist of the stem orientations from the initial ±25° of the α-phase crystal with respect to the thin film normal and possesses the [130] (or [$\bar{1}$30]) zone. Possible reasons for this 25° tilt within the *ac*-plane of the elongated α-phase crystals are discussed.

Acknowledgment. The authors would like to thank Dr. F. Khoury for helpful discussions. This work was supported by the National Science Foundation (DMR-0516602) and a graduate fellowship provided by the Chevron-Phillips Chemical Company and China Scholarship Council.

References and Notes

(1) Keith, H. D.; Padden, F. J.Jr; Walter, N. M.; Wickoff, H. W. *J. Appl. Phys.* **1959**, *30*, 1485.
(2) Addink, E. J.; Beintema, J. *Polymer* **1961**, *2*, 185.
(3) Khoury, F. A. *J. Res. Natl. Bur. Stand.* **1966**, *70A*, 29.
(4) Kardos, J. L.; Christiansen, A. W.; Naer, A. *J. Polym. Sci., A-2: Polym.* **1966**, *4*, 777.
(5) Binsbergen, F. L.; De Lange, B. G. M. *Polymer* **1968**, *9*, 23.
(6) Padden, F. J.Jr.; Keith, H. D. *J. Appl. Phys.* **1966**, *37*, 4013.
(7) Padden, F. J.Jr.; Keith, H. D. *J. Appl. Phys.* **1973**, *44*, 1217.
(8) Hikosaka, M.; Seto, T. *Polym. J.* **1973**, *5*, 111.
(9) Immirzi, A.; Iannelli, P. *Macromolecules* **1988**, *21*, 768.
(10) Natta, G.; Corradini, P. *Nuovo Cimento Suppl.* **1960**, *15*, 40.
(11) Meille, S. V.; Ferro, D. R.; Brükner, S.; Lovinger, A. J.; Padden, F. Jr. *Macromolecules* **1994**, *27*, 2615.
(12) Lotz, B.; Kopp, S.; Dorset, D. *C. R. Acad. Sci. Paris, Ser.IIb* **1994**, *319*, *187*.
(13) Lotz, B.; Graff, S.; Wittmann, J.-C. *J. Polym. Sci., Polym. Phys. Ed.* **1986**, *24*, 2017.
(14) Lotz, B.; Graft, S.; Straupé, C.; Wittmann, J.-C. *Polymer* **1991**, *32*, 2902.
(15) Corradini, P.; Petraccone, V.; Pirozzi, B. *Eur. Polym. J.* **1983**, *19*, 299.
(16) Sauer, J. A.; Pae, K. D. *J. Appl. Phys.* **1968**, *39*, 4959.
(17) Morrow, D. R. *J. Macromol. Sci., Phys. Ed.* **1968**, *B3*, 53.
(18) Brükner, S.; Meille, S. V.; Petraccone, V.; Pirozzi, B. *Prog. Polym. Sci.* **1991**, *16*, 361.
(19) Campbell, R. A.; Phillips, P. J.; Lin, J. S. *Polymer* **1993**, *34*, 4809.
(20) Mezghani, K.; Phillips, P. J. *Polymer* **1997**, *38*, 5725.
(21) Morrow, D. R.; Newman, B. A. *J. Appl. Phys.* **1968**, *39*, 4944.
(22) De Rosa, C.; Auriemma, F.; Circelli, T.; Waymouth, R. M. *Macromolecules* **2002**, *35*, 3622.
(23) Auriemma, F.; De Rosa, C. *Macromolecules* **2002**, *35*, 9057.
(24) De Rosa, C.; Auriemma, F.; Ruiz, O.; Resconi, L.; Camurati, I. *Macromolecules* **2007**, *40*, 6600.
(25) Brükner, S.; Meille, S. V. *Nature* **1989**, *340*, 455.
(26) Meille, S. V.; Brükner, S.; Porzio, W. *Macromolecules* **1990**, *23*, 4114.
(27) Hirose, M.; Yamamoto, T.; Naiki, M. *Comput. Theor. Polym. Sci.* **2000**, *10*, 345.
(28) Auriemma, F.; Ruiz, O.; De Rosa, C.; Corradini, P. *Macromolecules* **2000**, *33*, 8764.
(29) Stocker, W.; Magonov, S. N.; Cantow, H. J.; Wittmann, J.-C.; Lotz, B. *Macromolecules* **1993**, *26*, 5915.
(30) Lotz, B.; Wittmann, J.-C.; Lovinger, A. J. *Polymer* **1996**, *37*, 4979.
(31) Lotz, B.; Wittmann, J.-C. *J. Polym. Sci., Polym. Phys. Ed.* **1986**, *24*, 1541.
(32) Zhou, J. J.; Liu, J. G.; Yan, S. K.; Dong, J. Y.; Li, L.; Chan, C. M.; Schultz, J. M. *Polymer* **2005**, *46*, 4077.
(33) Janimak, J. J.; Cheng, S. Z. D.; Giusti, P. A. *Macromolecules* **1991**, *24*, 2253.
(34) Geil, P. H. *Polymer Single Crystals*; John Wiley & Sons: New York, **1963**.
(35) Cheng, S. Z. D. *Phase Transitions in Polymers: the Role of Metastable States*, Elsevier: Amsterdam, 2008.
(36) Wittmann, J.-C.; Lotz, B. *Makromol. Chim. Rapid Commun.* **1982**, *3*, 733.
(37) Wittmann, J.-C.; Lotz, B. *J. Polym. Sci., Polym. Phys. Ed.* **1985**, *23*, 205.
(38) Chen, J.; Cheng, S. Z. D.; Wu, S. S.; Lotz, B.; Wittmann, J.-C. *J. Polym. Sci., Polym. Phys. Ed.* **1995**, *33*, 1851.